Astron. Astrophys. 288, 697–704 (1994)

ASTRONOMY AND ASTROPHYSICS

Robust morphological measures for large-scale structure in the Universe

K.R. Mecke[1], T. Buchert[2], and H. Wagner[1]

[1] Sektion Physik der Universität München, Theresienstraße 37, D-80333 München, Germany
[2] Max-Planck-Institut für Astrophysik, Postfach 1523, D-85740 Garching, Germany

Received 16 December 1993 / Accepted 10 March 1994

Abstract. We propose a novel method for the description of spatial patterns formed by a coverage of point sets representing galaxy samples. This method is based on a complete family of morphological measures known as Minkowski functionals, which includes the topological Euler characteristic and geometric descriptors to specify the content, shape and connectivity of spatial sets.

The method is numerically robust even for small samples, independent of statistical assumptions, and yields global as well as local morphological information. We illustrate the method by applying it to a Poisson process, a 'double-Poisson' process, and to the Abell catalogue of galaxy clusters.

Key words: methods: statistical – cosmology: large-scale structure of universe

1. Introduction

Statistical measures provide important tools for the comparison of inhomogeneous cosmological models with observations of large–scale structure in the Universe. The discriminative power of this comparison depends chiefly on the statistical measure used. In the cosmological community the most frequently used measure was and still is the two-point correlation function of a point process such as the distribution of galaxies (e.g., Peebles 1980 and references therein; Davis & Peebles 1983), or clusters of galaxies (e.g., Bahcall & Soneira 1983). This measure appears to be crude: if we consider a cosmological density field, then the two-point correlation function only embodies information contained in the power spectrum of this field; it does not provide any information on the distribution of the phases of the Fourier components of the field, and it is limited to spatial regions which are well below currently observed large-scale structures such as, e.g., the "Great Wall" (Geller & Huchra 1989). As a consequence, completely different spatial patterns could display the same two-point correlation function (Martínez et al. 1990), i.e., no direct conclusions about the morphology of large-scale structure can be drawn. However, in general, the characteristics of the two-point correlation function as a small-scale measure are affected by the possible existence of large-scale inhomogeneities in an uncontrollable way. Moreover, they could depend strongly on 'biasing' assumptions about the relation between dark and luminous matter (Buchert & Martínez 1993; Martínez et al. 1994).

Efforts to go beyond the two–point correlation function comprise the consideration of higher–order correlations (Peebles 1980 and ref. therein), integrated unnormalized pair–counts (Mo et al. 1992), void probability functions (White 1979), percolation analysis (Shandarin 1983), minimal spanning trees (Barrow et al. 1985), Voronoi foam statistics (Icke & van de Weygaert 1987; van de Weygaert 1991), cell–count variance (Efstathiou et al. 1990), topological/geometrical structure discriminators (Mo & Buchert 1990), and multi–fractal measures (Martínez 1991). However, statistical measures which are sensitive to the morphology of structures have been investigated mostly in other fields such as image analysis and pattern recognition (Rosenfeld & Kak 1976 and ref. therein; Serra 1982). The reader may also consult the contributions (especially the survey articles by Barrow & Coles) in Feigelson & Babu (1992).

Of those approaches which focus on global aspects of the matter distribution, the use of topological descriptors appears to be among the most effective with respect to the comparison of cosmological theories and observations. Gott et al. (see the review by Melott 1990 and ref. therein) pursued this possibility and investigated methods to probe the topology of large–scale structure by employing the Euler characteristic or the genus of iso–density level surfaces of a density field obtained by smoothing the observed galaxy distribution. Recently, Brandenberger et al. (1994) modified this method into a *discrete genus statistic*.

This approach translates the phenomenology of the large–scale distribution of matter we observe in the Universe into a quantitative statement of connectedness of these structures: for different iso–density levels different topologies are realized by the same matter distribution. For high density levels isolated islands remain showing a *bubble* or *cluster* topology, for low

Send offprint requests to: T. Buchert

density levels a connected structure occurs which has the topology of a *honeycomb* or *swisscheese*, intermediate topologies are named *spongy*, i.e., holes and islands are interlocking (compare Melott 1988, 1990). Also, the change of the topology of large–scale structure can be an evolutionary effect: while the early distribution of QSO's exhibits a "bubble" topology, the evolution of overdense structures into interconnecting sheets of superclusters displays the opposite topology as is seen in the evolution of pancake models typical for a *HDM* (Hot–Dark–Matter) cosmogony.

The full morphological specification of spatial patterns requires *topological* as well as *geometrical* descriptors to characterize not only the connectivity but also the content and shape of figures. The aim of our paper is to point out that integral geometry supplies a suitable family of such descriptors, known as *Minkowski functionals*. In a d–dimensional ambient space there exist $d+1$ of these functionals. We are primarily interested in the case $d = 3$, where the Minkowski functionals are related with familiar measures: covered volume, surface area, integral mean curvature, and Euler characteristic. In a discussion remark Fred L. Bookstein (in: Feigelson & Babu 1992, pp. 49-55) has independently suggested the use of Minkowski functionals as possibly fruitful measures.

In order to apply the functionals to point–sets representing galaxy samples, we proceed by decorating each point with a spherical ball. The scale–dependent morphological features of this coverage may then be explored by varying the radius of the balls.

The Minkowski functionals are *global* and *additive* measures. Additivity allows us to calculate these measures effectively by summing up their *local* contributions, as in the case of the Euler characteristic. Moreover, the functionals are numerically *robust* against short–scale spatial irregularities in the coverage, which may arise via the variation of the ball radius. Finally, a further advantage is that the computation does not rely on statistical assumptions concerning the galaxy distribution.

In the next section we briefly review the mathematical background. In Sect. 3 the results of sample calculations are described. Sect. 4 gives a summary.

2. Minkowski functionals

Consider a set of points $\{x_i/i = 1,\dots,N\}$ which represent the positions of a sample of galaxies in three–dimensional Euclidean space $\mathbb{E}^3$. In order to study the global features of this point set, we introduce a collection of neighborhoods by covering each point with a spherical ball $B_r(x_i) = \{x \in \mathbb{E}^3/||\mathrm{x} - \mathrm{x_i}|| \leq \mathrm{r}\}$. For any chosen value of the radius r the union of these balls specifies an ensemble of clusters, where two balls are said to belong to the same cluster if they are connected by a chain of intersecting balls. By employing the Minkowski functionals to measure *content*, *shape* and *connectivity* of the covering $\mathscr{B}(r) = \cup_{i=1}^{N} B_r(x_i)$ under variation of r, we arrive at a quantitative operational definition for the scale–dependent morphological characteristics of the underlying spatial point process.

Since the methods of integral geometry are perhaps not widely known among physicists, we compile in this section some pertinent facts (Hadwiger 1957; Santaló 1976; Weil 1983).

The Minkowski functionals derive from the theory of convex sets. They generalize curvature integrals over smooth surfaces to the case of surfaces with singular edges and corners. In the example of the covering $\mathscr{B}(r)$ such irregularities arise from the intersections of the decorating balls.

Let K be a compact convex body in $\mathbb{E}^3$, with *regular* boundary $\partial K \in \mathscr{C}^2$ and principal radii of curvature R_1 and R_2. The surface area F of K is given by

$$F = \int_{\partial K} df = \int_{S^2} R_1 R_2 d\sigma \quad , \tag{1}$$

since the area element df on ∂K is related with the area element $d\sigma$ of the spherical image of ∂K under the Gaussian map by $df = R_1 R_2 d\sigma$.

Consider the convex body K_ϵ parallel to K at a distance ϵ, i.e.:

$$K_\epsilon = \cup_{x \in K} B_\epsilon(x) \quad . \tag{2}$$

Thus, the parallel body K_ϵ consists of all points within a distance $\leq \epsilon$ from K.
The radii of curvature of ∂K_ϵ are $R_1 + \epsilon$ and $R_2 + \epsilon$. Therefore

$$F_\epsilon = \int_{S^2} (R_1 + \epsilon)(R_2 + \epsilon) d\sigma = F + 2 \cdot H \cdot \epsilon + G \cdot \epsilon^2 \quad , \tag{3}$$

where

$$H = \frac{1}{2} \int_{\partial K} \left(\frac{1}{R_1} + \frac{1}{R_2} \right) df \tag{4}$$

is the *integral mean curvature* and

$$G = \int_{\partial K} \frac{1}{R_1 R_2} df \tag{5}$$

is the *integral Gaussian curvature* of ∂K.
If V denotes the volume of K and V_ϵ that of K_ϵ, we have

$$V_\epsilon = V + \int_0^\epsilon F_{\epsilon'} d\epsilon' = V + F \cdot \epsilon + H \cdot \epsilon^2 + \frac{4\pi}{3} \epsilon^3 \quad , \tag{6}$$

which is known as *Steiner's formula*.

More generally, Steiner's formula for convex bodies in d-dimensional Euclidean space may be written as

$$V_\epsilon(K) = \sum_{\alpha=0}^{d} \binom{d}{\alpha} W_\alpha(K) \epsilon^\alpha \quad , \tag{7}$$

whereby the Minkowski functionals $W_\alpha(K)$, $\alpha = 0,\dots,d$ are defined. For $d = 3$ we find by comparison

$$W_0(K) = V(K) \; , \quad 3W_1(K) = F(K) \; , \quad 3W_2(K) = H(K) \; ,$$

$$3W_3(K) = G(K) = 4\pi\chi(K) \quad , \tag{8}$$

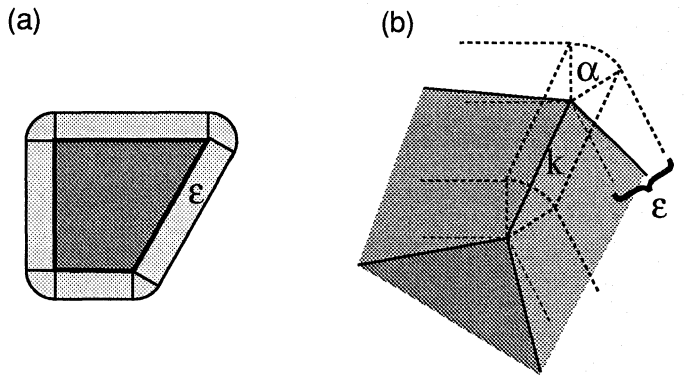

Fig. 1. a Parallel body of a convex polygone in $d = 2$. **b** The cylindrical segment at the edge k with dihedral angle α of a convex polyhedra contributes $\epsilon\alpha L$ to the parallel volume; therefore $3W_2(k) = \alpha L$

with the constant $\chi(K) = 1$ denoting the Euler characteristic of a convex body.

The expression (7) for $V_\epsilon(K)$ allows us to extend the definition of the functional W_α to any convex body without requiring regularity of ∂K; compare Fig.1. For example, let us take a cube Q in $\mathbb{E}^3$ with edge length a. Its parallel volume $V_\epsilon(Q)$ may be found by inspection,

$$V_\epsilon(Q) = a^3 + 6a^2\epsilon + 12a\frac{\pi}{4}\epsilon^2 + 8\frac{4\pi}{24}\epsilon^3 \quad . \tag{9}$$

The ϵ-terms are the contributions from the rectangular prisms on the faces of Q, from the cylindrical sectors on its edges and from the spherical sectors located on its corners.

Furthermore, Steiner's formula also yields the Minkowski functionals for lower dimensional ("improper") convex bodies embedded in $\mathbb{E}^d$, such as points, straight line segments, discs etc. .
For example, in the case of a disk D_r with radius r in $\mathbb{E}^3$ one finds

$$V_\epsilon(D_r) = 2\pi r^2\epsilon + \pi^2 r\epsilon^2 + \frac{4\pi}{3}\epsilon^3 \quad , \tag{10}$$

and thus

$$W_0(D_r) = V(D_r) = 0 \ , \ 3W_1(D_r) = F(D_r) = 2\pi r^2 \ ,$$
$$3W_2(D_r) = H(D_r) = \pi^2 r \ ,$$
$$3W_3(D_r) = G(D_r) = 4\pi\chi(D_r) = 4\pi \quad . \tag{11}$$

We note that the two–dimensional disk enters here as a cylindrical prism with vanishing height; therefore its "content" $F(D_r) = 2\pi r^2$ is twice the area of a two–dimensional ball with radius r. If $r \to 0$, the disk degenerates into a point $P = D_{r=0}$ with the Euler characteristic $\chi(P) = 1$ and $W_\alpha(P) = 0, \alpha = 0 \ldots d-1$.

Let us now list some common general properties of the functionals $W_\alpha : \mathscr{K} \to \mathbb{R}$. Here, $\mathscr{K}$ denotes the class of closed bounded convex subsets of $\mathbb{E}^d$.

Additivity : If $K \in \mathscr{K}$ is dissected by a planar cut into two convex parts such that $K = K_1 \cup K_2$, $K_1, K_2 \in \mathscr{K}$, then

$$W_\alpha(K_1 \cup K_2) = W_\alpha(K_1) + W_\alpha(K_2) - W_\alpha(K_1 \cap K_2) \ , \tag{12}$$

holds for each $\alpha = 0, \ldots, d$.

This relation is easily verified if $K = B_r(x)$ is a ball in $\mathbb{E}^3$ which is cut into two hemispheres K_1 and K_2. For instance, the surface area $(4\pi r^2)$ of $K_1 \cup K_2$ is obtained by adding up the surface areas of the hemispheres $(2 \cdot (2\pi r^2 + \pi r^2))$ and subtracting the area $(2\pi r^2)$ of the disk $D_r = K_1 \cap K_2$.

Motion invariance : Let $\mathscr{G}$ be the group of motions (translations and rotations) in $\mathbb{E}^d$. The transitive action of $g \in \mathscr{G}$ on $K \in \mathscr{K}$ is denoted by gK. Then

$$W_\alpha(gK) = W_\alpha(K) \ ; \alpha = 0 \ldots d \ , \tag{13}$$

i.e., the Minkowski functionals of a body are independent of its location in space.

Continuity : If $K_n \to K$ for $n \to \infty$, $K_n, K \in \mathscr{K}$ (with convergence defined in terms of the Hausdorff metric for sets), then

$$W_\alpha(K_n) \to W_\alpha(K) \ ; \alpha = 0 \ldots d \ . \tag{14}$$

Intuitively, this continuity property expresses the fact that an approximation of a convex body by convex polyhedra K_n, for example, also yields an approximation of $W_\alpha(K)$ by $W_\alpha(K_n)$.

So far we only considered the Minkowski functionals restricted to the class $\mathscr{K}$ of convex bodies. Since we want to apply these measures to investigate the spatial pattern of coverage models as described at the beginning of this section, the definition of the Minkowski functionals must be extended to non–convex sets such as $\mathscr{B}(r)$. This extension may be achieved in the following way (Hadwiger 1957):

Let $\mathscr{R}$ denote the class of subsets of $\mathbb{E}^d$ which can be represented as a finite union of sets from $\mathscr{K}$, i.e., $A \in \mathscr{R}$ if and only if $A = \cup_{i=1}^N K_i$, $N < \infty$, $K_i \in \mathscr{K}$. The class $\mathscr{R}$ also includes the empty set $\emptyset$. In the first step, the Euler characteristic is introduced by

$$\chi(A) = \begin{cases} 1 & , \quad A \in \mathscr{K} \ , \ A \neq \emptyset \ , \\ 0 & , \quad A = \emptyset \ . \end{cases} \tag{15}$$

and extended to $\mathscr{R}$ via additivity,

$$\chi(A \cup B) = \chi(A) + \chi(B) - \chi(A \cap B) \tag{16}$$

for any $A, B \in \mathscr{R}$. In particular,

$$\chi(\cup_{i=1}^N K_i) = \sum_i \chi(K_i) -$$
$$\sum_{i<j} \chi(K_i \cap K_j) + \ldots + (-1)^{N+1}\chi(K_1 \cap K_2 \cap \ldots \cap K_N) \ , \tag{17}$$

which follows from eq. (12) by induction. The right–hand side of eq. (17) only involves convex sets and may be applied together with eq. (15) to compute $\chi(A)$ for any $A \in \mathscr{R}$, as illustrated in Fig.2. We also note that $\chi : \mathscr{R} \to \mathbb{Z}$ is motion invariant and it can be shown to agree with the Euler characteristic as defined in algebraic topology. In the cosmology literature (e.g. Melott 1990) the Euler characteristic is usually associated with

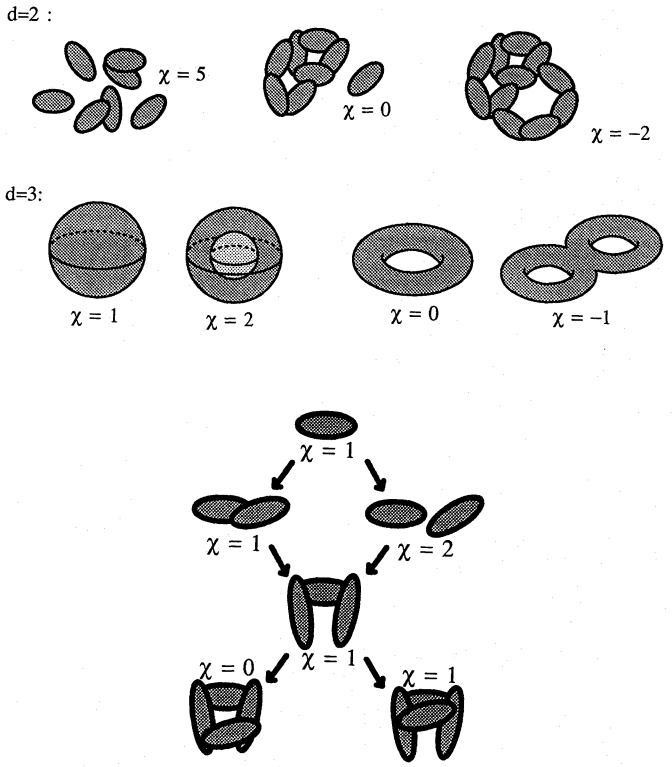

Fig. 2. Illustrative examples of the Euler characteristic in two and three dimensions. In two dimensions χ is the difference of components and holes, whereas in three dimensions it is the sum of the disconnected components and cavities minus the number of tunnels. A negative Euler characteristic indicates network–like structures. Bottom: Illustrative calculation of χ using additivity

the surface ∂A of a body A. For closed $(d-1)$-dimensional smooth surfaces in $\mathbb{E}^d$ one has the simple relationship

$$\chi(\partial A) = \chi(A)\left(1+(-1)^{d-1}\right) \ . \tag{18}$$

As a second step of the extension, the Minkowski functionals are defined for $A \in \mathscr{R}$ by

$$W_\alpha(A) = \int \chi(A \cap E_\alpha) d\mu(E_\alpha) \quad , \quad \alpha = 0, \ldots, d-1 \ ,$$

$$W_d(A) = \omega_d \chi(A) \quad , \quad \omega_d = \pi^{d/2}/\Gamma(1+d/2) \ . \tag{19}$$

Here, E_α is a $\alpha-$dimensional plane in $\mathbb{E}^d$. The integral runs over all positions (induced by translations and rotations) of E_α, weighted with the so–called kinematical density $d\mu(E_\alpha)$ (Hadwiger 1957; Santaló 1976) which is related to the invariant Haar measure on the group of motions $\mathscr{G}$ and is normalized such that for a d–dimensional ball B_r with radius r, $W_\alpha(B_r) = \omega_d r^{d-\alpha}$. The volume of the unit ball $(B_{r=1})$ is ω_d.

In the case of convex $A \in \mathscr{K}$ the Eq. (19) reproduce the Minkowski functionals obtained previously from $V_\epsilon(A)$ (e.g. Miles 1974).

According to their definition (19), the Minkowski functionals on $\mathscr{R}$ inherit from the Euler characteristic the property of additivity, i.e.,

$$W_\alpha(\cup_{i=1}^N K_i) = \sum_i W_\alpha(K_i) -$$

$$\sum_{i<j} W_\alpha(K_i \cap K_j) + \ldots + (-1)^{N+1} W_\alpha(K_1 \cap \ldots \cap K_N) \ , \tag{20}$$

as well as motion invariance. These features together with their "conditional continuity" (the W_α are continuous when restricted to $\mathscr{K}$) specify the Minkowski functionals as a distinguished family of geometrical and topological descriptors: There is a remarkable theorem (Hadwiger 1957) which asserts that any additive, motion invariant and conditionally continuous functional $\mathscr{F}$ on subsets $A \subset \mathbb{E}^d$, $A \in \mathscr{R}$, is a linear combination of the $d+1$ Minkowski functionals,

$$\mathscr{F}(A) = \sum_{\alpha=0}^{d} c_\alpha W_\alpha(A) \ , \tag{21}$$

with real coefficients c_α independent of A. Important consequences of this theorem are the "principal kinematical formulae", which may be written concisely in the form

$$\int_{\mathscr{G}} M_\alpha(A \cap gB) dg = \sum_{\beta=0}^{\alpha} \binom{\alpha}{\beta} M_{\alpha-\beta}(B) M_\beta(A)$$

$$M_\alpha(A) = \frac{\omega_{d-\alpha}}{\omega_\alpha \omega_d} W_\alpha(A) \ , \quad \alpha = 0, \ldots, d \ . \tag{22}$$

The integral is performed with respect to the invariant Haar measure dg of $\mathscr{G}$ and runs over all motions of the set B, with $A, B \in \mathscr{R}$. In the case $B = B_\epsilon(x)$ and $A = K \in \mathscr{K}$ the kinematical formula for $\alpha = d$ reproduces Steiner's formula (7),

$$\int_{\mathbb{R}^d} \chi(K \cap B_\epsilon(x)) d^d x = V_\epsilon(K) \ . \tag{23}$$

The kinematic formulae are useful mathematical tools in stereology and stochastic geometry. The Minkowski functionals can be calculated efficiently for any given coverage without requiring statistical assumptions about the underlying point set. However, when the latter constitutes a realization of a random spatial process (which is the case in cosmological models for structure formation) then one faces a difficult problem: to infer the statistics of random geometrical patterns from a generally limited amount of point set data. It turns out that the mean values of the Minkowski functionals provide *unbiased stereological estimators* (Weil 1983). Moreover, these mean values can be calculated exactly for the classical Boolean model (Mecke & Wagner 1991), where the centers of balls are distributed in $\mathbb{E}^d$ according to Poisson's law, which is often employed as a reference model.

For convenience, we recall the result for these mean values per ball B_r and for $d = 3$:

$$< \frac{V}{N} >= \frac{1}{\rho}(1 - e^{-\nu}) \ , \tag{24a}$$

$$< \frac{F}{N} >= 4\pi r^2 e^{-\nu} \ , \tag{24b}$$

$$< \frac{H}{N} >= 4\pi r(1 - \frac{3\pi^2}{32}\nu)e^{-\nu} \ , \tag{24c}$$

$$< \frac{G}{N} >= 4\pi < \chi >= 4\pi(1 - 3\nu + \frac{3\pi^2}{32}\nu^2)e^{-\nu} \ , \tag{24d}$$

with $\nu = 4\pi r^3\rho/3$ and the number density ρ of balls.

In the general case where the statistics of a point set in a domain $\subset \mathbb{E}^3$ with volume Ω is specified by a sequence of density correlation functions $\{\rho_n(x_1, \ldots, x_n) | n = 1, 2, \ldots\}$, the mean values for the augmented coverage per unit volume are obtained from the additivity relation (20) in the form

$$< \frac{1}{\Omega} W_\alpha[\mathscr{B}(r)] >= \sum_{n=1}^{\infty} \frac{(-1)^{n+1}}{n!\Omega} \int \cdots \int_\Omega \rho_n(y_1, \ldots y_n) \cdot$$

$$\cdot W_\alpha[\cap_{i=1}^n B_r(y_i)] d^3y_1 \ldots d^3y_n \ . \tag{25}$$

Obviously, the Minkowski functionals embody information from every order n of the correlations.

3. Examples

In this section we calculate the Minkowski functionals for three examples of point processes in $\mathbb{E}^3$: a Poisson process, a 'double-Poisson' process and the ACO–catalogue of galaxy clusters.

3.1. Calculation method

The Minkowski functionals $W_\alpha[\mathscr{B}(r)]$ for a covering $\mathscr{B}(r) = \cup_{i=1}^N B_r(x_i)$ of a given point set $\{x_1, \ldots, x_N\} \subset \mathbb{E}^3$ may be calculated straightforwardly via the additivity relation (20). However, in the cases $\alpha \geq 1$ this algorithm becomes inefficient when the amount of overlap between the augmented balls is excessive, since one has to compute many redundant and mutually cancelling terms. Therefore, we proceed, for $\alpha \geq 1$, alternatively as follows (Mecke 1993):

The covering $\mathscr{B}(r)$ divides the whole space by piecewise smooth spherical contours. These pieces are joined along circular arcs where two balls intersect, and at singular points (vertices) which have equal distance to the centers of three balls. Configurations where four or more arcs have a point in common carry negligible weight and can be ignored. Consider a ball $B_r(x_i)$ which is only partially covered by other balls. The area F_i and the integral curvatures H_i and G_i of the uncovered surface part S_i are given by

$$F_i = \int_{S_i} df = 3W_1(S_i) \ , \quad H_i = \frac{1}{r}F_i = 3W_2(S_i) \ ,$$

$$G_i = \frac{1}{r^2}F_i = 3W_3(S_i) \ . \tag{26}$$

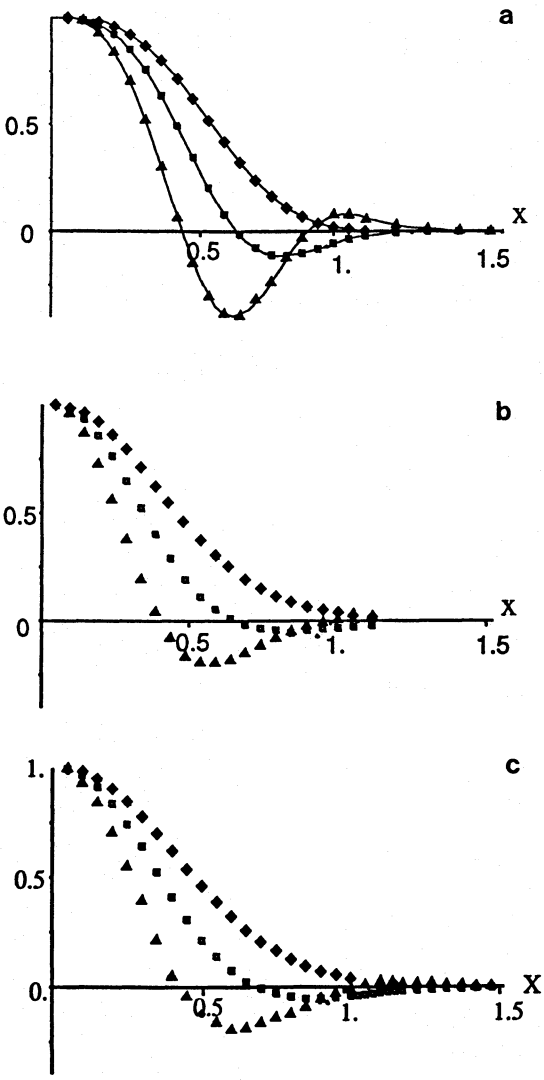

Fig. 3. Mean values of the Minkowski functionals, i.e., of the reduced surface area $\Phi_1(x)$ (diamonds), the reduced integral mean curvature $\Phi_2(x)$ (rectangles), and the reduced Euler characteristic $\Phi_3(x)$ (triangles) are depicted for a Poisson-process (3a), a 'double-Poisson' process (3b) and the ACO-catalogue (3c). The curves in Fig. 3a are obtained from the analytical formulas (Eq. (24)). The measures are normalized to 1 at $x = 0$ and the radius x of the balls centered at each point of the process is measured in units of the mean distance $\rho^{-1/3}$ of the points, where ρ is the number density of the process

An uncovered arc A_{ij} which length ℓ_{ij} on the intersection $B_r(x_i) \cap B_r(x_j)$, $\|x_i - x_j\| = a_{ij} < 2r$, gives rise to the curvature contributions

$$H_{ij} = \frac{1}{2}\alpha_{ij}\ell_{ij} = 3W_2(A_{ij}) \ ,$$

$$G_{ij} = \frac{a_{ij}\ell_{ij}}{r\sqrt{r^2 - (a_{ij}/2)^2}} = 3W_3(A_{ij}) \ , \tag{27}$$

where α_{ij} denotes the angle between the normals of $B_r(x_i)$ and $B_r(x_j)$ along A_{ij}.

The Gaussian curvature $G_{ijk} = 3W_3(P_{ijk})$ at an uncovered vertex P_{ijk} on the common intersection of three balls centered

at x_i, x_j, x_k equals the solid angle spanned by the three normals of the balls at P_{ijk} and is obtained from l'Huilier's formula

$$[\tan(\frac{1}{4}G_{ijk})]^2 = \tan(\frac{\alpha_1+\alpha_2+\alpha_3}{4})\tan(\frac{\alpha_1+\alpha_2-\alpha_3}{4})\cdot$$
$$\cdot\tan(\frac{\alpha_1-\alpha_2+\alpha_3}{4})\tan(\frac{-\alpha_1+\alpha_2+\alpha_3}{4}) ,$$
$$\sin(\frac{\alpha_1}{2}) = \frac{\|x_i-x_j\|}{2r} , \sin(\frac{\alpha_2}{2}) = \frac{\|x_i-x_k\|}{2r} ,$$
$$\sin(\frac{\alpha_3}{2}) = \frac{\|x_j-x_k\|}{2r} . \quad (28)$$

Finally, the total values of $W_\alpha[\mathscr{B}(r)]$ are given by

$$W_1[\mathscr{B}(r)] = \sum_i W_1(S_i) ,$$
$$W_2[\mathscr{B}(r)] = \sum_i W_2(S_i) - \sum_{ij} W_2(A_{ij}) ,$$
$$W_3[\mathscr{B}(r)] = \sum_i W_3(S_i) - \sum_{ij} W_3(A_{ij})$$
$$+\sum_{ijk} W_3(P_{ijk}) = 4\pi\chi[\mathscr{B}(r)] , \quad (29)$$

where the sums run over all uncovered surface pieces, arcs and vertices.

In the figures below we display the reduced values of the Minkowski functionals $\Phi_\alpha = W_\alpha[\mathscr{B}(r)]/NW_\alpha(B_r)$, where N is the number of sample points, and $W_\alpha(B_r) = \frac{4\pi}{3}r^{d-\alpha}, d = 3$; in particular, $\Phi_3 = \chi[\mathscr{B}(r)]/N$.

As a consequence of the additivity of Minkowski functionals, the statistical errors are always smaller than the graphical symbols used in the figures. The computation time on a local PC requires a few CPU–seconds for a sample of hundred points, increasing nearly linearly with the number of points N.

In the equations (29) the global Minkowski functionals are expressed in terms of *local* measures. The latter also allow us to introduce individual Minkowski functionals $W_\alpha(x_i; r)$ for each ball $B_r(x_i)$(=: B_i, for short). in the following way:

$$W_\alpha(x_i; r) = W_\alpha(S_i) - \frac{1}{2}\sum_{j,j\neq i} W_\alpha(A_{ij})\chi(B_i\cap B_j)$$
$$+\frac{1}{3}\sum_{j<k,j,k\neq i} W_\alpha(P_{ijk})\chi(B_i\cap B_j\cap B_k) . \quad (30)$$

The Euler characteristics in Eq. (30) equal unity if the convex intersections are non–empty and vanish otherwise. The factors $1/2$ and $1/3$ arise, since an arc and a vertex are shared by two and three balls, respectively. Moreover, $W_1(A_{ij}) = W_1(P_{ijk}) = W_2(P_{ijk}) = 0$. These individual local measures (30) provide means for defining subsamples by selecting for fixed r those balls whose associated measures attain values in a prescribed interval. Examples are shown in Fig.6 below.

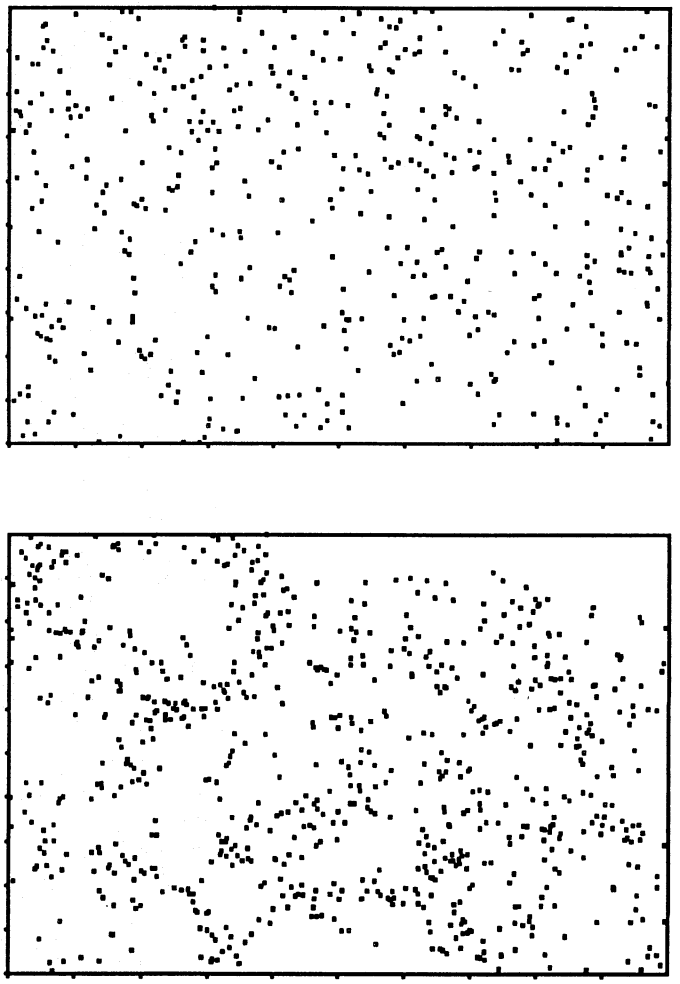

Fig. 4. Thin planar slices from a three-dimensional cube: the upper panel shows 500 points which are independently distributed (Poisson-process); the lower panel shows 750 points which are distributed according to the 'double-Poisson' process as explained in Sect. 3.3

3.2. *Poisson process*

In the first example the coverage $\mathscr{B}(r)$ is based on 10^4 points, independently distributed in a unit cube with number density ρ. We use the length scale $x = \rho^{1/3}r$, normalized by the mean distance of the points; thus, the edge–length of the cube is $x_{\text{cube}} = 21.6$. The radius of the decorating balls is varied within the interval $0 \leq x \leq 1.6$; its maximum value is small enough compared with x_{cube} to avoid finite–size effects.

Fig.3a displays the values of $\Phi_\alpha(x), 1 \leq \alpha \leq 3$. The curves are the mean values $< \Phi_\alpha(x) >$ as obtained from Eq. (24). For small radii, $\mathscr{B}(r)$ consists of isolated balls with negligible overlap; therefore, each measure starts out at unity. As the overlap increases, the measures decrease together with the reduced total surface area $\Phi_1(x)$ of the coverage. $\Phi_2(x)$ changes its sign, since the curvature of the singular edges at intersections is negative and starts to dominate the positive contribution from the spherical parts of the surface as the overlap increases. Negative values of the Euler characteristic $\Phi_3(x)$ are typical for a highly connected, "sponge-like" structure with many tunnels. We also

note that the first zero of $\Phi_3(x)$ at $x_p \approx 0.44$ provides a reliable estimate for the percolation threshold in the continuum in comparison with simulation data (Mecke & Wagner 1991).

3.3. 'Double–Poisson' process

This process was implemented as follows: 50 centers of spherical shells were randomly placed in a unit cube. Then, 200 points were distributed independently within each shell. The resulting total number of points in the cube turned out to be 6841. The edge–length of the cube was $x_{\text{cube}} = 19.0$, the inner and the outer radius of each shell has been chosen as $x_i = 3.4$ and $x_o = 3.8$.

Fig.4 presents the projections of 750 points from a thin planar slice cut out from the cube. For comparison, we also show a two–dimensional Poisson process with 500 points.

The measures $\Phi_\alpha(x)$ for the 'double–Poisson' process are given in Fig.3b. In comparison with Fig.3a, the $x-$range with negative Euler characteristic is extended: As x increases, the balls start to overlap earlier and they fill the space later. This feature is also reflected in the filaments and bigger voids recognizable in Fig.4. The minimum value of the Euler characteristic is higher than in the pure Poisson case, indicating that now the structure is less "spongy" with fewer (but bigger) tunnels.

3.4. ACO–catalogue

For the third example of a point process we take the ACO-catalogue of galaxy clusters (Abell et al. 1989, see also Postman et al. 1992 and the recent paper on the topological characterization of the catalogue by Rhoads et al. 1994). We consider a spherical section of the northern hemisphere with an opening angle of 120^o and a radius of 450 h^{-1}Mpc or $z = 0.15$. Each cluster in this section is taken into account, but we neglect thinning in distance and other possible deviations from a 'fair sample'. In this way we obtain 923 clusters of galaxies; the radius of the section is $x_{\text{section}} = 9.6$ in normalized units, again big enough to avoid edge effects, as in the previous examples. Since the clusters are already extended objects, the ball radii are chosen such that $x \geq 0.06$ ($r_{\text{cluster}} \geq 3$ h^{-1}Mpc). In Fig.3c the Minkowski measures for the coverage of this observed point process are plotted.

To exhibit the significance of these measures we display in Fig.5 the data for the Euler characteristic per unit surface area $\chi^*(x) := \chi(x)/F(x)$ for the three examples. The enhancement of $\chi^*(x)$ at larger radii results from the reduction of the size of uncovered tunnels. The similarity between the data obtained from the ACO–catalogue and those from the 'double-Poisson' process is remarkable in view of the fact that the parameters chosen in the latter have not been adjusted or optimized.

In Fig.6 we show planar projections of three–dimensional ACO–subsamples selected by the values of the individual Euler characteristics of partially covered balls, as described in Sect. 3.1. Only the centers of the balls are displayed.

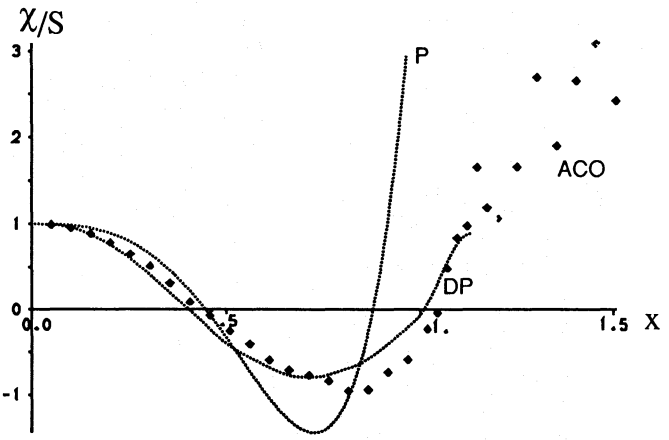

Fig. 5. The mean Euler characteristic per surface area $\chi^*(x)$ for the three point processes discussed: a Poisson–process (P), a 'double–Poisson' process (DP), and the ACO–catalogue (ACO). The zeros near $x_p = 0.44$ indicate similar percolation thresholds. The discrepancy of (P) and (ACO) obviously rules out the Poisson–process as a statistical model, whereas the similarity of (DP) and (ACO) is remarkable

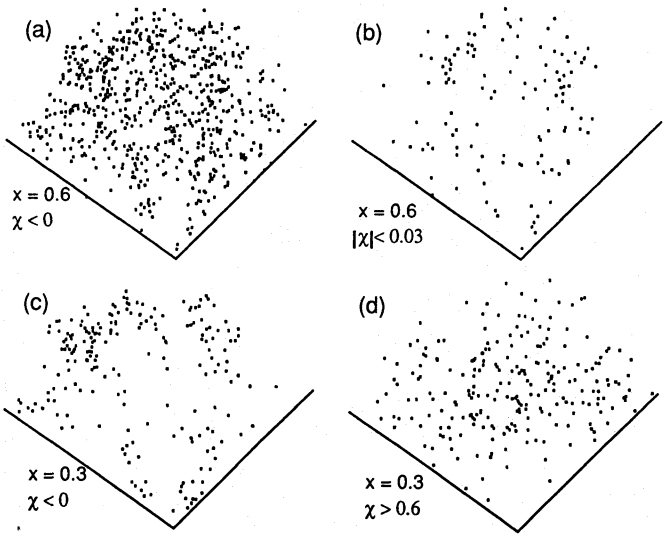

Fig. 6. Subsamples from the ACO–catalogue with the individual Euler characteristic χ of each ball (with reduced radius x) as selection criterion, projected onto a plane. This illustrates the possibility to classify cluster environments by using the concept of *local morphology* introduced in this work

4. Concluding remarks

We have presented a method to analyze the spatial patterns of galaxy distributions by employing the Minkowski functionals which provide a complete family of morphological measures. In order to apply this concept to the point–set representing a sample of galaxies, we introduced a coverage by marking each member of the point–set with the center of a ball. The common radius of the balls is used as a diagnostic parameter for displaying the morphological features of the coverage on different length–scales, i.e., with varying spatial resolution. In three–dimensional space

the family of Minkowski measures consists of the Euler characteristic, the covered volume, the surface area of the coverage, and its integral mean curvature.
The important aspects of the method may be summarized as follows.

• On the practical side, the calculation of the Minkowski functionals is *precise* and *CPU time effective*. In contrast to the currently popular approach (see, e.g., Melott 1990) for measuring the Euler characteristic (or the genus $g = 1 - \chi$) of iso–density contours which requires the choice of two parameters, namely a smoothing length and a density level, the present method only involves the radius of the covering balls as a *single* scale.

• As a consequence of their additivity, the Minkowski functionals are *robust* and *global* measures: They yield stable results even for small samples.

• The method is efficient in *discriminating* different spatial patterns. Moreover, the method does not depend on assumptions about the statistics of patterns, or model realizations, respectively.

• The *mean* values of the Minkowski functionals provide *statistically unbiased* descriptors which contain features of n–point correlation functions at *any* order n. Therefore, the present method is complementary to the conventional approach restricted to low–order correlation functions.

Finally, the stereological properties of Minkowski functionals (see, e.g., Weil 1983) offer means to infer morphological characteristics of three–dimensional samples from lower–dimensional sections such as "pencil beams" or two–dimensional all–sky surveys. These stereological applications as well as a more detailed statistical analysis is postponed to future work.

The numerical code to realize the Minkowski functionals is available via e–mail: TOB @ mpa-garching.mpg.de

Acknowledgements. We would like to thank John A. Peacock for providing us the new Abell cluster catalogue, and Jürgen Ehlers as well as the referees for valuable remarks on the manuscript. TB is supported by DFG (Deutsche Forschungsgemeinschaft).

References

Abell G.O., Corwin H.G., Olowin R.P. (1989): ApJS **70**, 1
Bahcall N.A., Soneira R.M. (1983): ApJ **270**, 20
Barrow J.D., Bhavsar S.P., Sonoda D.H. (1985): MNRAS **216**, 17
Brandenberger R.H., Kaplan D.M., Ramsey S.A. (1994): MNRAS, submitted
Buchert T., Martínez V.J. (1993): ApJ **411**, 485
Davis M., Peebles P.J.E. (1983): ApJ **267**, 465
Efstathiou G., Kaiser N., Saunders W. et al. (1990): MNRAS **247**, 10
Feigelson E., Babu G.J. (1992) (eds.): *Statistical Challenges in Modern Astronomy*, Springer, New York
Geller M.J., Huchra J.P. (1989): Science **246**, 887
Hadwiger H. (1957): *Vorlesungen über Inhalt, Oberfläche und Isoperimetrie*, Springer, (in German)
Icke V., van de Weygaert R. (1987): A&A **184**, 16
Martínez V.J., Jones B.J.T., Dominguez-Tenreiro R., van de Weygaert R. (1990): ApJ **357**, 50
Martínez V.J. (1991): in: *Applying Fractals to Astronomy*, Lecture Notes in Physics, eds.: A. Heck, J. Perdang, Springer, pp. 135-159
Martínez V.J., Portilla M., Jones B.J.T., Paredes S. (1994): A&A **280**, 5
Mecke K.R., Wagner H. (1991): J. Stat. Phys. **64**, 843
Mecke K.R. (1993): Ph.D.–Thesis, University of Munich (in German)
Melott A.L. (1988): GRG **21**, 495
Melott A.L. (1990): Phys. Reports **193**, 1
Miles R.E. (1975): Adv. Appl. Prob. **7**, 818
Mo H.J., Buchert T. (1990): A&A **234**, 5
Mo H.J., Deng Z.G., Xia X.Y., Schiller P., Börner G. (1992): A&A **257**, 1
Peebles P.J.E. (1980): *The Large–scale Structure of the Universe*, Princeton Univ. Press
Postman M., Huchra J.P., Geller M.J. (1992): ApJ **384**, 404
Rhoads J.E., Gott III J.R., Postman M. (1994): ApJ, in press
Rosenfeld A., Kak A.C. (1976): *Digital Picture Processing*, Academic Press
Santaló L.A. (1976): *Integral Geometry and Geometric Probability*, Addison-Wesley
Serra J. (1982): *Image Analysis and Mathematical Morphology* **Vol.1,2**, Academic Press
Shandarin S.F. (1983): Sov. Astron. Lett. **9**, 104
Van de Weygaert R. (1991): Ph.D.–Thesis, Leiden University
Weil W. (1983): *Stereology*, in: *Convexity and its Applications*, eds.: Gruber P.M., Wills J.M., Birkhäuser
White S.D.M. (1979): MNRAS **186**, 145

This article was processed by the author using Springer-Verlag TEX A&A macro package 1992.